

Effects of Symmetry Energy on the Equation of State for Hybrid Neutron Stars

Parada T. P. Hutaaruk,^{1,2} Hana Gil,^{2,3} Seung-il Nam,^{1,3,4} and Chang Ho Hyun^{2,3}

¹*Department of Physics, Pukyong National University (PKNU), Busan 48513, Korea*

²*Department of Physics Education, Daegu University, Gyeongsan 38453, Korea*

³*Center for Extreme Nuclear Matters,
Korea University, Seoul 02841, Korea*

⁴*Asia Pacific Center for Theoretical Physics (APCTP), Pohang 37673, Korea*

(Dated: July 19, 2023)

Abstract

In this paper, the implications of the symmetry energy on the hadron and quark phase transitions in the compact star, including the properties of the possible configurations of the quark-hadron hybrid stars, are investigated in the frameworks of the energy-density functional (EDF) models and the flavor SU(2) Nambu–Jona-Lasinio (NJL) model with the help of the Schwinger’s covariant proper-time regularization (PTR) scheme. In this theoretical setup, the equations of states (EoSs) of hadronic matter for various values of symmetry energies obtained from the EDF models are employed to describe the hadronic matter, and the flavor SU(2) NJL model with various repulsive-vector interaction strengths are used to describe the quark matter. We then observe the obtained EoS in the mass-radius properties of the hybrid star configurations for various vector interactions and nuclear symmetry energies by solving the Tolman-Oppenheimer-Volkoff equation. We obtain that the critical density at which the phase transition occurs varies over the density $(3.6\text{--}6.7)\rho_0$ depending on the symmetry energy and the strength of the vector coupling G_v . The maximum mass of the neutron star (NS) is susceptible to G_v . When there is no repulsive force, the NS maximum mass is only about $1.5M_\odot$, but it becomes larger than $2.0M_\odot$ when the vector coupling constant is about half of the attractive scalar coupling constant. Surprisingly, the presence of the quark matter does not affect the canonical mass of NS ($1.4M_\odot$), so observing the canonical mass of NSs can provide unique constraints to the EoS of hadronic matter at high densities.

I. INTRODUCTION

A key question about the composition of matter at densities several times the nuclear saturation density (ρ_0) is how it differs from the state that constitutes the atomic nuclei. It was widely known that several exotic states are candidates for the states of matter at ultra-high densities: The creation of hyperons, the onset of Bose-Einstein condensates, and transformation to quark matter. Using theories of subatomic physics, one can estimate in what conditions the new state of matter will emerge. However, the existence of the new state matter is not yet established, for instance, the appearance of the hyperons and Δ baryon in the matter and how they interact with other matter constituents are still open questions.

In a recent work of Ref. [1], the in-medium interaction of the Λ hyperon was investigated within non-relativistic nuclear density functional theory. Parameters for the interaction of Λ hyperon were determined to reproduce the single- Λ hypernuclear data, and the effect of the density dependence of the symmetry energy was examined in more systematic detail. It was shown that the density at which Λ hyperons appear depends strongly on the symmetry energy. However, the appearance density of hyperons is always larger than $3\rho_0$, so the hyperon is not likely to affect the properties of a canonical mass ($1.4M_\odot$) of NS because the density at the center of the NS canonical mass is generally less than $3\rho_0$. Kaon condensation was also considered in the relativistic and non-relativistic models [2, 3]. Unless the interaction of the kaon in dense nuclear matter is super-strongly attractive, the formation of the kaon condensation is less probable.

Analogously, the matter composition in NSs naively can be illustrated as the quarks in the baryons on a microscopic scale. In the bag model, baryons are described as spherical bags in which quarks are assumed to be confined. In the bag model, the charge radius of the proton is expected around 0.6 – 0.8 fm (corresponding to the volume 0.9 – 2.1 fm³). The inverse of the number density (ρ) is the volume occupied by a nucleon. If $\rho_0 = 0.16 \text{ fm}^{-3}$, one nucleon occupies 6.25 fm³ at the saturation density. This volume is larger than the volume of a nucleon, so nucleons are separated spatially. At densities in the range of 3 – 6 ρ_0 , the volume per nucleon becomes equal to the volume of a nucleon, so the nucleons begin to overlap each other. As the matter density evolves above the onset of overlapping, nucleons overlap more, and it becomes vague to define the confinement of a quark in a specific bag. Matter transforms to the phase of deconfined quarks. A similar condition is expected to

occur in NS.

Given the equation of state (EoS) of dense matter, one can calculate the bulk properties of the NSs such as mass, radius, and particle distribution in the core by solving the Tolman-Oppenheimer-Volkoff (TOV) equations. With the nuclear models that are well constrained by the nuclear properties and nuclear matter properties from the heavy ion collision experiments, *ab initio* calculations, and modern neutron star observation data [4–9], the density at the center of a canonical mass of NS is obtained to be about or less than $3\rho_0$, and that of the heaviest stars ($\geq 2M_\odot$) is around $6\rho_0$. The degrees of freedom that constitute the core of NSs might likely change from hadron to quarks in NSs with masses in the range $(1.4 - 2.0)M_\odot$.

The main issue of the present work is to explore the uncertainty of the critical density (ρ_c) at which the transition from the hadronic phase to the deconfined quark matter begins and its impact on the properties of the NS. For this purpose, for the EoS of hadronic matter (HM), we employ the KIDS (Korea-IBS-Daegu-SKKU) energy density functional (EDF) in which the density dependence of the symmetry energy is calibrated to the radius of $1.4M_\odot$ mass NSs in the range $R_{1.4} = 11.8 - 12.5$ km [8]. The KIDS0, KIDS-A, KIDS-B, KIDS-C, and KIDS-D models, as well as the standard Skyrme SLy4 model used in the work, have distinctive density dependence of the symmetry energy, so the results will provide the range of ρ_c within the uncertainty of the nuclear matter EoS. On the quark matter (QM) side, the proper time NJL model is used for the EoS of the deconfined quark state. As discussed above, massive NSs are likely to have a QM phase in the core, so we investigate the range of parameters in the NJL model that are compatible with the NS mass larger than $2M_\odot$. As a result, we can determine the ranges of the parameters in the QM EoS. Combining the EoSs of the KIDS model with those of the NJL model, we determine the range of ρ_c from the condition $P_{\text{HM}}(\rho_c) = P_{\text{QM}}(\rho_c)$ at $\rho_{\text{HM}} = \rho_{\text{QM}} = \rho_c$, where P_{HM} , P_{QM} , ρ_{HM} , and ρ_{QM} represent the pressure in the hadronic phase, pressure in quark phase, density in hadronic phase, and density in quark phase, respectively. The results will shed light on (i) the effect of the symmetry energy on the change of phase in the NS core, (ii) consistency of the hybrid models with the NS properties determined from astronomical observations, and (iii) uncertainty of the EoS in the hadronic and quark phases.

This work is organized as follows. In Sec. II, models for the hadronic matter and deconfined quark matter are briefly introduced. The hadronic matter is described in the

KIDS-EDF model, whereas the quark matter is described in the flavor SU(2) Nambu–Jona-Lasinio model with the help of the Schwinger proper-time regularization scheme, that is so-called NJLPTR model. We present and discuss the numerical result of the current work in Sec. III, and we summarize the work in Sec. IV.

II. FORMALISM FOR THE HADRON AND QUARK PHASES

A. Hadronic matter from the KIDS functional

In this section, we first present the description of HM in the KIDS-EDF model [4, 10, 11]. This model was constructed based on the Fermi momentum expansion, which is relevant for infinite nuclear matter (INM) and an NS. The energy per particle for homogeneous hadronic matter in the powers of the cubic root of the density is given by

$$\mathcal{E}_{\text{HM}}(\rho, \delta) = \mathcal{T}(\rho, \delta) + \sum_{j=0}^3 (\alpha_j + \beta_j \delta^2) \rho^{(1+j/3)}, \quad (1)$$

where $\mathcal{T}(\rho, \delta)$ is the kinetic energy. $\delta = (\rho_n - \rho_p)/\rho$ and $\rho = \rho_n + \rho_p$ are respectively the isospin asymmetry and baryon density. The α_j and β_j are respectively the coefficients for the symmetric and antisymmetric nuclear matter.

The symmetry energy $S(\rho)$ is straightforwardly determined through the second derivative of the energy per particle with respect to δ at the nuclear saturation density. It then gives

$$\mathcal{E}_{\text{HM}}(\rho, \delta) = \mathcal{E}(\rho, 0) + S(\rho) \delta^2 + \mathcal{O}(\delta^4), \quad (2)$$

$$S(\rho) = \frac{\hbar}{6M} \left(\frac{3\pi^2}{2} \right)^{2/3} \rho^{2/3} + \sum_{j=0}^3 \beta_j \rho^{(1+j/3)}, \quad (3)$$

where $M \equiv (M_n + M_p)/2$ is the nucleon mass in free space. The pressure for the HM can be calculated from the energy per particle with respect to baryon density. It then has the form

$$P_{\text{HM}} = \rho^2 \frac{\partial \mathcal{E}_{\text{HM}}(\rho, \delta)}{\partial \rho}. \quad (4)$$

Here we emphasize again that, in this work, the HM is represented by the five KIDS-EDF models: KIDS0, KIDS-A, KIDS-B, KIDS-C, and KIDS-D models, and the Skyrme force

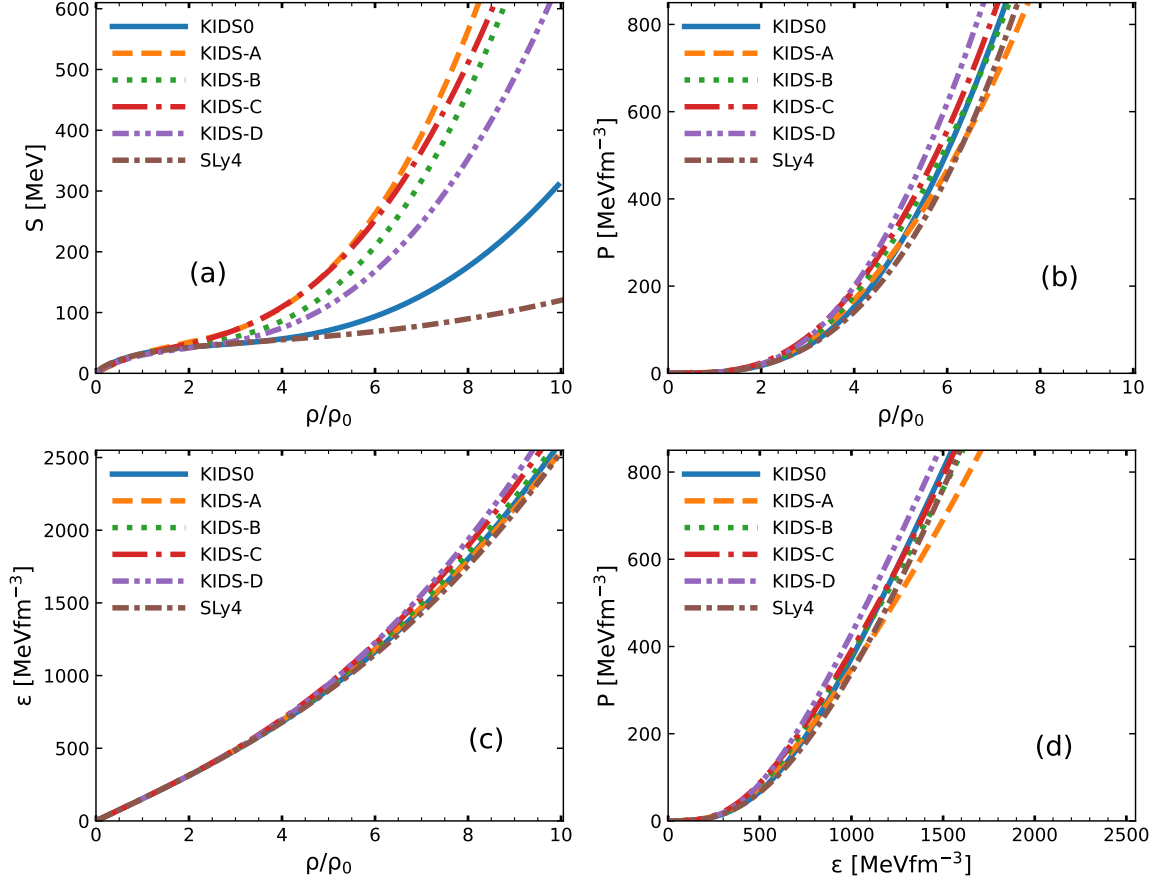


FIG. 1: From the KIDS EDFs and the SLy4 model: (a) Symmetry energy, (b) Pressure of HM as a function of ρ/ρ_0 , (c) Energy density of HM as a function of ρ/ρ_0 and (d) EoS of HM.

SLy4 model. Those various EDF models have different nuclear symmetry energies, which cover soft to stiff nuclear symmetry energies. The nuclear symmetry energy results for the KIDS0, KIDS-A, KIDS-B, KIDS-C, KIDS-D, and SLy4 models are given in Fig. 1 (a). It clearly shows different ranges of symmetry energies covering soft and stiff symmetry energies that will be used to construct the EoS of the hybrid model. Figure 1 (a) shows, for HM, the stiffest symmetry energy is given by the KIDS-A model, and the softest is given by the SLy4 model. We also provide the pressure of the NS matter as a function of the densities in Fig. 1 (b). The pressures of the symmetric matter obtained from the EDF models are consistent with the heavy-ion collision (HIC) reaction data at high density [12] as well as the chiral perturbation theory (ChPT) at low density [13].

The result for the energy densities E_{HM} of the NS matter for the hadronic models with respect to density is given in Fig. 1 (c). Results for the $P_{\text{HM}}-E_{\text{HM}}$ relation for the hadronic

models are shown in Fig. 1 (d). This EoS relation is required as input for calculating the TOV equation to obtain the properties of the NSs. In the HM model, we found that the M_{NS}/M_{\odot} results for the KIDS0 and SLy4 models are rather similar because both models have soft symmetry energies. In contrast, the KIDS-A and KIDS-B models have stiff symmetry energies giving a larger radius of the NS. Overall, the mass and radius of NS results for all KIDS models fit well with the recent observations [14–16].

B. Pure quark matter from the NJLPTR model

In this section, we describe the pure (nonstrange) quark matter (PQM) in the framework of the flavor SU(2) Nambu–Jona-Lasino (NJL) model [17–26]. This model is built in terms of the quark degrees of freedom in the form of the four-fermion contact interactions. Therefore, this model is very suitable and powerful for the description of quark matters. The general NJL Lagrangian density for two quark flavors can be written as

$$\mathcal{L}_{\text{NJL}} = \bar{\psi}_q (i\not{\partial} - \hat{m}_q) \psi_q + G_s [(\bar{\psi}_q \psi_q)^2 + (\bar{\psi}_q \gamma_5 \vec{\tau} \psi_q)^2] - G_\omega (\bar{\psi}_q \gamma_\mu \psi_q)^2 - G_\rho (\bar{\psi}_q \gamma_\mu \vec{\tau} \psi_q)^2, \quad (5)$$

where the quark field is given by $\psi_q = (\psi_u, \psi_d)^T$, $\vec{\tau}$ stands for the Pauli isospin matrices, and $\hat{m}_q = \text{diag}[m_u, m_d]$ is the current (bare) quark mass, where, in this work, we use the isospin symmetry, giving $m_u \simeq m_d$. The G_s , G_ω , and G_ρ are respectively scalar, isoscalar-vector, and isovector-vector coupling constants. Note that the NJL model suffers the divergence in the quark propagator, therefore, we must apply a regularization scheme to cure the divergence problem. In this work, we perform the PTR scheme to tame the divergence [27]. In the standard NJL formalism, the effective quark mass can be easily obtained in the mean-field approximation (MFA), which is explicitly given in the PTR scheme as

$$M_q = m_q - 2G_s \langle \bar{\psi}_q \psi_q \rangle = m_q + \frac{3G_s M_q}{\pi^2} \int_{\Lambda_{\text{UV}}^{-2}}^{\infty} d\tau \frac{\exp[-\tau M_q^2]}{\tau^2}, \quad (6)$$

where $\langle \bar{\psi}_q \psi_q \rangle$ is the chiral condensate for flavor q , which relates to the order parameter of the spontaneous breaking of chiral symmetry (SB χ S). It is worth noting that the effective quark mass in Eq. (6) has an additional correction in the quark matter, which comes from

the density term in the quark propagator.

In the QM, the NJL Lagrangian density in Eq. (5) is modified by adding an extra term of quark density or quark operator chemical potential. It then has the form

$$\mathcal{L}_{\text{NJL}} \rightarrow \mathcal{L}_{\text{NJL}} + \bar{\psi}_q \hat{\mu}_q \gamma^0 \psi_q, \quad (7)$$

where $\hat{\mu}_q = \text{diag}[\mu_u, \mu_d]$ is the quark chemical potential matrix. Thus, considering the density effect, the quark propagator for flavor q in momentum space can be written by

$$S_q(p) = \frac{1}{[(p_0 + \tilde{\mu}_q) \gamma^0 - \vec{p} \cdot \vec{\gamma} - M_q]}, \quad (8)$$

where the $\tilde{\mu}_q$ is the so-called the reduced quark chemical potential for flavor q and it can be written as

$$\tilde{\mu}_q = \mu_q - 2G_v \rho_q^v, \quad (9)$$

where $\rho_q^v \simeq \langle \psi_q^\dagger \psi_q \rangle = p_{F_i}^3 / \pi^2$ stands for the individual quark number densities of flavor q , where p_{F_i} is the Fermi momentum for quark flavor $i = (u, d)$. For simplicity, in the present work, we opt the vector coupling $G_v = G_\omega = G_\rho$ by considering vector dominance and small mass differences between ρ and ω masses [28, 29]. Also, it is worth noting that the G_v will be treated as a free parameter in this work.

In the standard method, the effective potential for the nonstrange QM in the NJL model is given by [30]

$$\begin{aligned} \mathcal{V}_{\text{NJL}}^{\text{QM}}(M_q, \mu_q) &= 2iN_c \sum_{q=[u,d]} \int \frac{d^4k}{(2\pi)^4} \log \left[\frac{k^2 - M_q^2 + i\epsilon}{k^2 - M_0^2 - i\epsilon} \right] \\ &+ \sum_{q=[u,d]} \frac{(M_q - m_q)^2}{8G_s} - \sum_{q=[u,d]} \frac{(M_0 - m_q)^2}{8G_s} \\ &- 2N_c \sum_{q=[u,d]} \int \frac{d^3k}{(2\pi)^3} \Theta(\tilde{\mu}_q - E_q(k)) [\tilde{\mu}_q - E_q(k)] - \sum_{q=[u,d]} \frac{V_0^2}{8G_v}, \end{aligned} \quad (10)$$

where the first term has divergence, therefore it has to be regularized using the PTR scheme. The reduced quark chemical potentials for u and d quarks are defined by $\tilde{\mu}_u = \tilde{\mu}_d =$

$\mu_u - 2G_v\rho_u^v$, as also given in Eq. (9). $V_0 = 2G_v\langle\psi_q^\dagger\psi_q\rangle$, $E_u(k) = E_d(k) = \sqrt{\vec{k}^2 + M_0^2}$, and M_0 are the vector field (potential), quark energy, and the constituent quark mass in free space, respectively. We note that we have subtracted a constant (free space) contribution ($M_q = M_0$) in the effective potential in Eq. (10). Therefore pressure becomes zero in free space. Along with this effective potential definition and the so-called Gibbs-Duhem relation, the energy density will also vanish in free space [31].

Using the effective potential in Eq. (10) the pressure and the energy density for the normal (nonstrange) QM are respectively expressed by

$$P_{\text{QM}} = -\mathcal{V}_{\text{NJL}}^{\text{QM}}(M_q, \mu_q) - \mathcal{V}_l(\mu_l), \quad E_{\text{QM}} = \mathcal{V}_{\text{NJL}}^{\text{QM}}(M_q, \mu_q) + \sum_{q=[u,d]} \mu_q \rho_q^v, \quad (11)$$

$$\rho_q = -\frac{\partial \mathcal{V}_{\text{NJL}}^{\text{QM}}(M_q, \mu_q)}{\partial \mu_q}. \quad (12)$$

In the calculation of the QM EoS, the NJL parameters have been fitted to the pion mass $m_\pi = 0.14$ GeV, and the pion weak decay constant $f_\pi = 0.093$ GeV, giving $G_s = 3.17$ GeV⁻² and $\Lambda_{\text{UV}} = 1.0789$ GeV. The constituent quark mass $M_0 = 0.20$ GeV and the current quark mass $m_q = 0.0055$ GeV, which is similar to PDG values [32]. Results for the effective quark mass, pressure, and energy density of the quark matter for vector interaction couplings $G_v = (0.00, 0.25, 0.50)G_s$ are shown in Fig. 2. As expected, the effective quark masses decrease as the density increases as shown in Fig. 2 (a). Additionally, the effective quark mass is not sensitive to the change of the values of the vector repulsive interaction coupling, where the rate of change is slightly low. This effective quark mass result is consistent with the result obtained in Refs. [21, 30].

Results for the pressure of the PQM are given in Fig. 2 (b). It shows that the pressure is stiffer with a larger value of G_v . Such behavior is a natural and expected result because a larger G_v value makes the repulsive force become stronger. In addition, we show the results for the E - ρ relation of the PQM for different values of G_v in Fig. 2 (c). A similar result with the pressure is found: The energy density increases as the G_v value and density increase, which can be clearly understood from the relation of $P_{\text{QM}} = -\mathcal{V}_{\text{NJL}}^{\text{QM}} - \mathcal{V}_l$ and $E_{\text{QM}} = \mathcal{V}_{\text{NJL}}^{\text{QM}} + \sum_q \mu_q \rho_q^v$, as given in Eq. (11). It implies that increasing the value of pressure is only given by increasing the energy density (increasing $-E$) and *vice versa*, as explained in the visualization of Fig. 12 of Ref. [21]. Figure 2 (d) shows EoS P - E relation for different

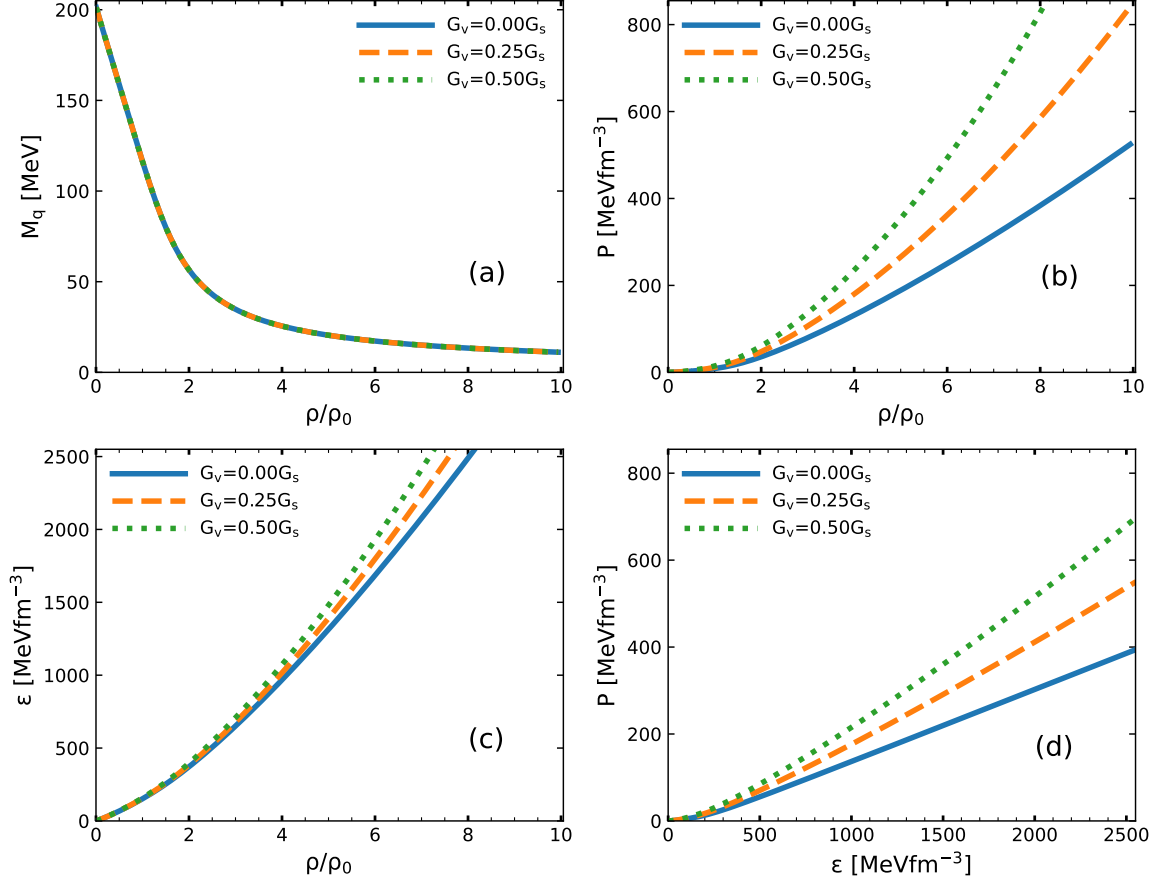


FIG. 2: From the NJLPT model: (a) Effective quark mass for different values of G_v as a function of ρ/ρ_0 , (b) Pressure of QM as a function of ρ/ρ_0 , (c) Energy density of QM as a function of ρ/ρ_0 , and (d) EoS of PQM.

values of G_v . We found that the pressure increases as the energy density and G_v increase. This also indicates that the EoS of the QM is stiffer for higher values of G_v .

C. Properties of the static hybrid star

Here, we input the obtained EoSs for hadronic and quark matters for different values of G_v and symmetry energies into the TOV equation to numerically compute the properties of a non-rotating NS, obtaining the mass-radius (M-R) relation (structure of the hybrid star). The TOV equations are given by [33–35]

$$\frac{dP(r)}{dr} = -\frac{G[E(r) + P(r)][M(r) + 4\pi r^3 P(r)]}{r[r - 2GM(r)]}, \quad \frac{dM(r)}{dr} = 4\pi r^2 E(r), \quad (13)$$

where $P(r)$ and $E(r)$ are respectively the pressure and energy density at radial position r . G and $M(r)$ are the gravitational constant and mass within the sphere of radius r , respectively. Using the EoSs of the constructed hybrid stars as input, we obtain the M - R relation as a result. Note that the EoSs of the hybrid stars are depicted in Fig. 3.

III. NUMERICAL RESULT

A. Critical density of the hybrid star

In this section, we present the results of the critical densities of the phase transition of the hadronic to the quark matter for different KIDS models and the Skyrme model. The critical density ρ_c is simply determined by finding the cross point between P_{HM} and P_{QM} . It is also worth noting that the ρ_c is the phase transition from the hadronic and quark phases that occurs when $P_{\text{HM}}(\rho_c) = P_{\text{QM}}(\rho_c)$ and $\rho_{\text{HM}} = \rho_{\text{QM}}$. In Fig. 3, it shows P_{HM} for each hadronic model and P_{QM} with three values of the vector coupling constant $G_v = 0, 0.25G_s,$ and $0.5G_s$. Figure 3 (a) shows P_{HM} for the KIDS0 model and P_{QM} for the NJL model with different values of G_v . The critical density for P_{HM} and P_{QM} for $G_v = 0.00G_s$ is around $\rho_c = 3.60\rho_0$. The ρ_c increases as the value of G_v increases. The ρ_c for the KIDS-A model is shown in Fig. 3 (b). Note that the KIDS-A model has stiffer symmetry energy than that for the KIDS0 model. The critical density for the KIDS-A model and the NJL model with $G_v = 0.00G_s$ and $G_v = 0.25G_s$ are smaller than those for the KIDS0 model. However, the critical density for the KIDS-A model and the NJL model with $G_v = 0.5G_s$ is larger than that obtained for the KIDS0 model. This feature is followed by the KIDS-B, KIDS-C, and KIDS-D models as shown in Figs. 3 (c)-(e), while the SLy4 model and the NJL model with different values of G_v almost have similar critical density values as those for the KIDS0 model and the NJL model with the corresponding values of G_v . This can be understood because both KIDS0 and SLy4 models have softer nuclear symmetry energies in comparison to other KIDS models as shown in Fig. 1. For all the hadronic models and the NJL model with different G_v values, the EoS is stable in the hadron phase at low densities, and the QM becomes more stable than the HM at high densities.

Again, comparing the ρ_c values for larger values of $G_v = 0.5G_s$ among the KIDS-A, KIDS-B, KIDS-C, and KIDS-D models, the highest value of ρ_c is given by the KIDS-A model,

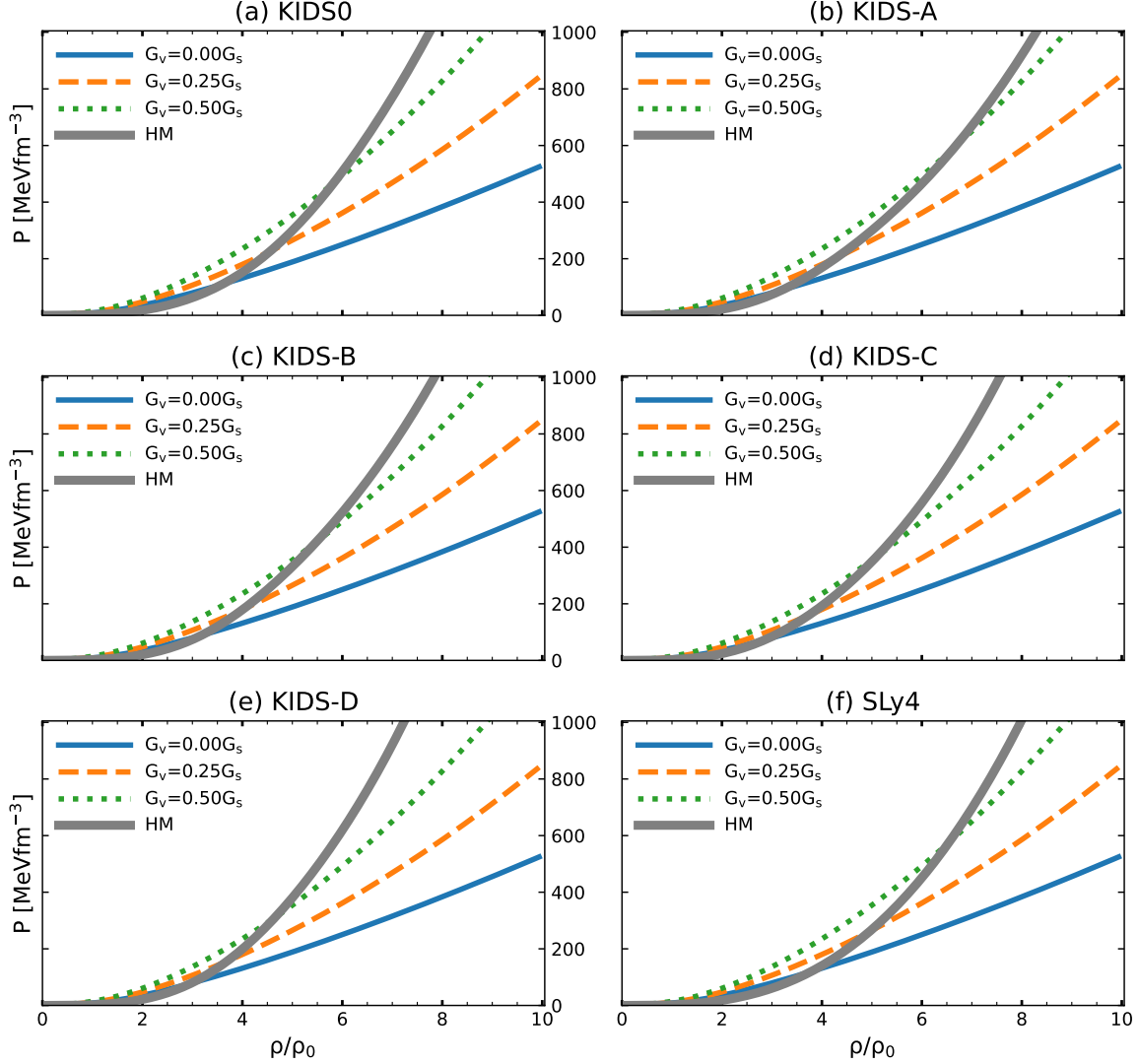


FIG. 3: Pressure as a function of density for QM with different values of G_v and for HM in the different EDF models: (a) KIDS0, (b) KIDS-A, (c) KIDS-B, (d) KIDS-C, (e) KIDS-D, and (f) SLy4. The critical density ρ_c is given by the cross point between P_{HM} and P_{QM} with different values of G_v . The thick solid line is P - ρ relation for HM. The thin solid line is P - ρ relation for QM with $G_v = 0.00G_s$, the dashed line is P - ρ relation for QM with $G_v = 0.25G_s$, and the dotted line is P - ρ relation for QM with $G_v = 0.50G_s$.

and it decreases in the order of KIDS-B, KIDS-C, and KIDS-D models. The ordering of ρ_c could be understood from the stiffness of symmetry energy. With a soft symmetry energy (small L and K_{sym} values, where L and K_{sym} are respectively the slope and the curvature of symmetry energies), the energy to create a neutron becomes small, so the β -equilibrium condition allows easy creation of the neutron, which eventually leads to a large fraction of

TABLE I: Transition point obtained from the P - ρ/ρ_0 relation for the hybrid KIDS-NJLPTR models with different values of G_v . The units of the coupling constants of G_v and G_s are MeV^{-2} , and P is $\text{MeV}\cdot\text{fm}^{-3}$. Note that ρ_c is in the unit of ρ_0 .

G_v	KIDS0	KIDS-A	KIDS-B	KIDS-C	KIDS-D	SLy4
	(P_c, ρ_c)	(P_c, ρ_c)	(P_c, ρ_c)	(P_c, ρ_c)	(P_c, ρ_c)	(P_c, ρ_c)
$0.00G_s$	(110.23, 3.60)	(89.98, 3.21)	(88.21, 3.18)	(73.00, 2.86)	(78.15, 2.97)	(119.73, 3.78)
$0.25G_s$	(226.44, 4.55)	(203.39, 4.29)	(181.44, 4.02)	(159.28, 3.74)	(155.71, 3.69)	(261.06, 4.95)
$0.50G_s$	(464.75, 5.81)	(592.96, 6.65)	(417.06, 5.47)	(365.00, 5.09)	(309.08, 4.65)	(574.79, 6.54)

the neutron. Pauli blocking makes the pressure exerted by the neutron strong when there are more neutrons within the neutron star. For this reason, the pressure becomes stiff from KIDS-A to KIDS-D while the symmetry energy is stiffened in the reverse order. Exact values of ρ_c are summarized in Tab. I. One can see that, regardless of G_v value, the transition to the quark phase occurs at low densities with soft symmetry energy. Values of the pressure at ρ_c (P_c) are also summarized in the table.

Overall, it indicates that the phase transition is highly sensitive to both the nuclear symmetry energy in the hadron phase and the vector repulsion in the quark phase. Their effect on physical observables can be probed by solving the TOV equations and obtaining the mass and radius of neutron stars.

B. M - ρ and M - R relations of the hybrid star

Figure 4 displays the mass of an NS as a function of the density at the center. For the pure hadronic matter, all six models produce the NS maximum masses (M_{max}) greater than $2M_{\odot}$. The NS maximum mass for the KIDS-D model is the largest as shown in Fig. 4 (e), and it decreases in the order of KIDS-C, KIDS-B, and KIDS-A models as in Figs. 4 (b)-(d). This result is consistent with the stiffness of EoS in Fig. 1. The result changes dramatically if QM exists in the core of the star.

The thick solid lines denote the NS mass results of the hadronic matter as in Fig. 4 (a)-(f). In all the hybrid KIDS-NJL models, the density at which the thin solid lines begin is equal to ρ_c in Tab. I, which means that as the transition to quark matter occurs, the EoS becomes soft then the matter cannot support strong gravity. As a result, M_{max} is determined at the density of phase transition. For $G_v = 0$, ρ_c is not much sensitive to the models, so

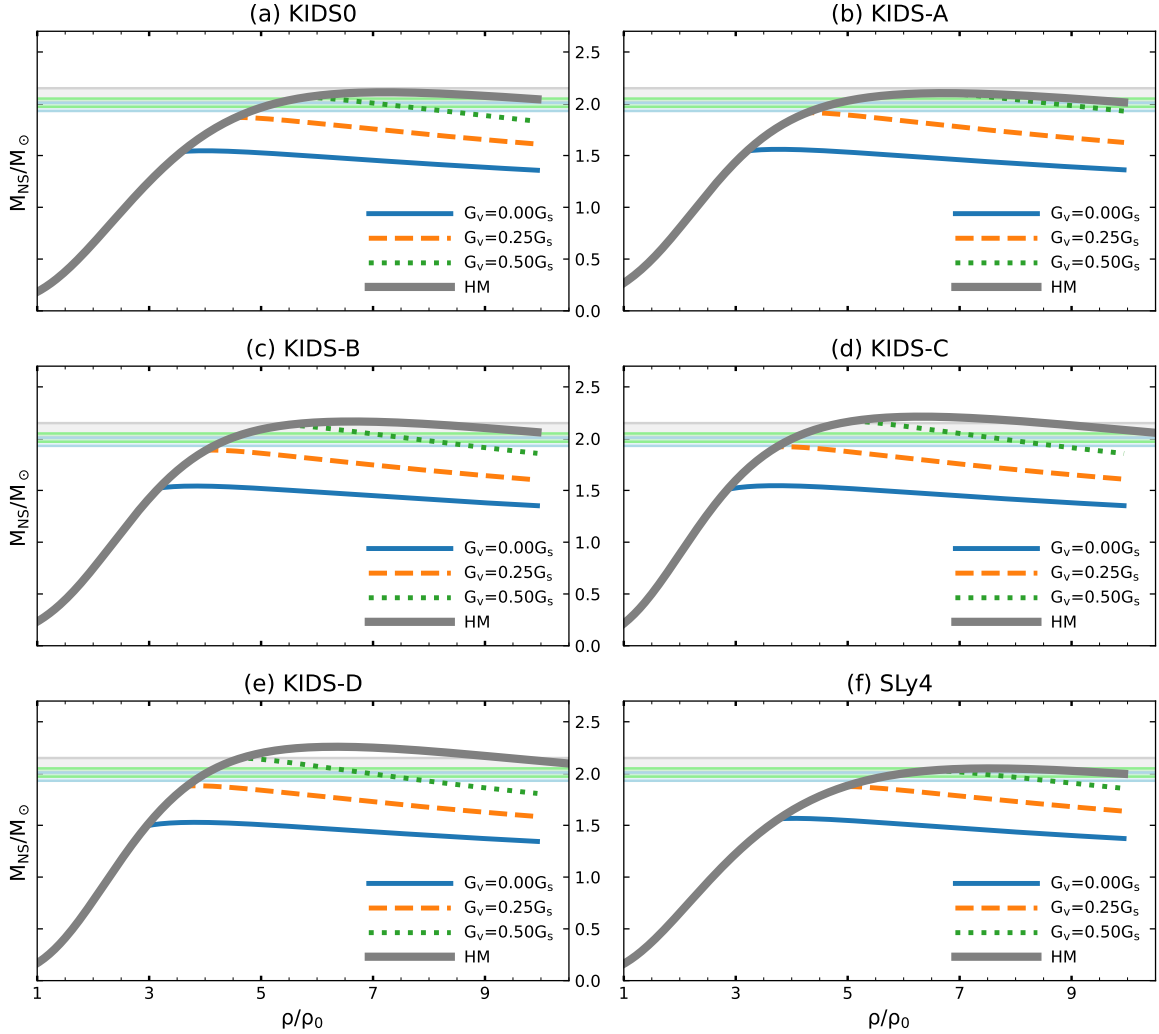


FIG. 4: NS mass-density relations of different hadron-quark matter EoS with different values of G_v for different EDF models: (a) KIDS0, (b) KIDS-A, (c) KIDS-B, (d) KIDS-C, (e) KIDS-D, and (f) SLy4. The thick solid line represents the NS mass for the HM. The thin solid line is the NS mass for the HM+QM with $G_v = 0.00G_s$, the dashed line is the NS mass for the HM+QM with $G_v = 0.25G_s$, and the dotted line represents the NS mass for the HM+QM with $G_v = 0.50G_s$.

the NS maximum masses are obtained in a narrow range $(1.5\text{--}1.6)M_\odot$. These values are substantially low in comparison to $2M_\odot$, so the result confirms that vector repulsion must be necessarily accounted for in the QM to reproduce the observation of the large mass of NS. The dashed lines correspond to the result of $G_v = 0.25G_s$ as shown in Fig. 4 (a)-(f). Similar to $G_v = 0$, the density at which a dashed line begins is the same with ρ_c in Tab. I, and M_{\max} is determined at the density where the mass is below $2M_\odot$ for all EDF models. The result demands that the G_v must be higher than $0.25G_s$.

The results of $G_v = 0.5G_s$ which are shown with dotted lines are now consistent with the $2M_\odot$ constraint. The density at which the QM curve begins is the highest is given by the KIDS-A model, and it then decreases in the order of KIDS-B, KIDS-C, and KIDS-D models. This ordering is understood easily in terms of the stiffness of the EoS of each model. Contrary to the results of $G_v = 0$ and $0.25G_s$, the density at which the dotted curves begin is higher than the ρ_c values in Tab. I. The difference means that even after the QM is formed in the core, its EoS is stiff enough that it can resist gravitational contraction up to a certain density, at which the NS star reaches the maximum value. However, the interval between ρ_c and the density at the maximum mass of NS is narrow, so the fraction of QM in the core of the NS is not likely to be significant. Summarizing the result, to satisfy the $2M_\odot$ condition, the G_v value must be larger than a certain value to obtain the QM EoS stiff. The stiff QM EoS increases ρ_c , and the high ρ_c value constrains the existence of QM in a limited range.

Figure 5 presents the mass-radius (M - R) relation obtained from the TOV equations. Since the data from GW and NICER provide information on both mass and radius of NS, they can constrain the EoS of HM and QM more strictly than the data of mass alone. The radius of NS canonical mass ($1.4M_\odot$) $R_{1.4}$ is of particular interest and importance. According to the NICER analysis [38], the NS radius is $R_{1.4} = 12.45 \pm 0.65$ km within 1σ credible interval [38]. On the theoretical side, the density at the center of $1.4M_\odot$ NS is obtained not to exceed $3\rho_0$ in general. The density at which exotic states such as the mixture of the hyperon or transition to QM appear is above $2\rho_0$ as a whole, though the uncertainty is non-negligible. Therefore, the properties of $1.4M_\odot$ NS are especially important to probe (i) the EoS of HM at high densities if there is no transition to QM or hyperon, or (ii) consistency of the EoS of exotic phases with the data of $1.4M_\odot$ NS if these exotic states exist in the interior of the $1.4M_\odot$ NS. The M - R result shows that the effect of QM appears at NS masses higher than $1.5M_\odot$, so the radius of $1.4M_\odot$ NS is unaffected by the transition to QM. Hyperon is another source that can soften the EoS of $1.4M_\odot$ NS. According to work in progress [39], if the $\Lambda\Lambda$ interaction determined from the experimental data of double- Λ hypernuclei is included in the EoS of hyperon matter, it makes the EoS stiff. As a consequence, the maximum mass of the NS becomes larger than $2M_\odot$, and the creation of the hyperon gives negligible effect to the radius of $1.4M_\odot$ star. Therefore, accurate measurement of $R_{1.4}$ can provide stringent constraints on the EoS of HM at densities up to $3\rho_0$.

In comparison with other results, our results show the difference to some extent, but

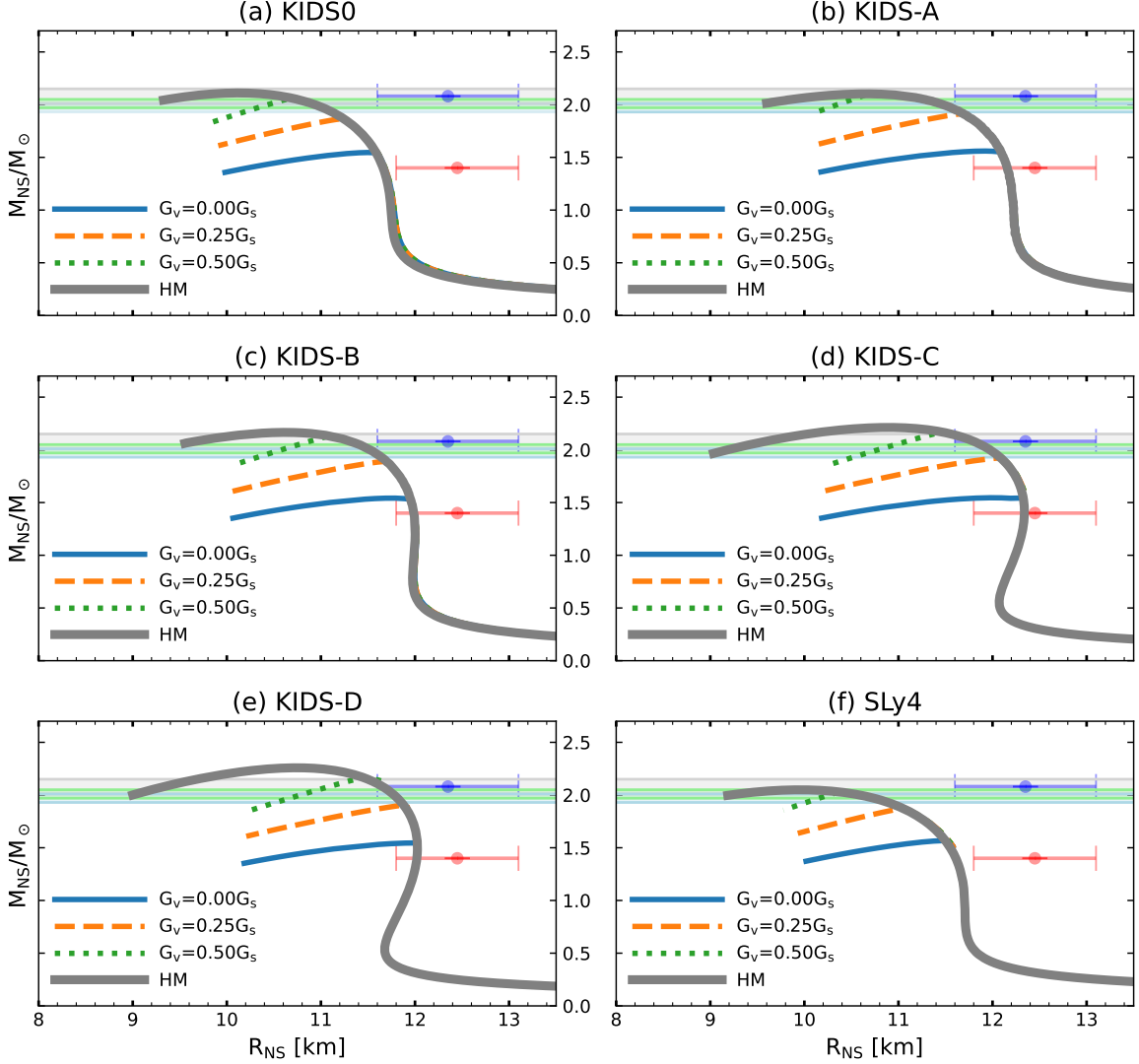


FIG. 5: Same as Fig. 4, but for NS M - R relations. Horizontal error bars show the radius of $1.4M_{\odot}$ and $2.08M_{\odot}$ stars determined in the NICER analysis [38].

qualitatively both results are compatible. In works of Refs. [40, 41], they reported that transition or crossover to QM is considered. In both works, QM was described in terms of the NJL model, but for the HM, an RMF model is used in [40], and a chiral effective field theory (χ EFT) and Togashi EoSs are employed in [41].

In Ref. [40], the result of the MS-B+vNJL model is comparable to our work. Three values are assumed for the vector repulsion of QM, $G_v/G_s = 1.5, 2.0,$ and 2.5 . The result shows that the NS maximum mass is below $2M_{\odot}$ when $G_v = 1.5G_s$, and it becomes obviously above $2M_{\odot}$ when $G_v = 2.0G_s$. It is notable that, in our calculation, $M_{\max} \geq 2M_{\odot}$ is obtained

if $G_v \geq 0.5G_s$, so there is a huge difference in the strength of the vector repulsion. M - R curve of MS-B+vNJL is also very different from what we obtain. Transition to QM occurs at $\rho = 1.5\rho_0$ or $\rho = 2.0\rho_0$ in the MS-B+vNJL model, and then the radius becomes smaller than the radius of the HM. The radius of the $1.4M_\odot$ NS is about 12.5 km without QM, but it falls in the range 11.7–12.2 km depending on the G_v and ρ_c values. Radii of the maximum mass NSs are located below 11 km, which is much smaller than the NICER estimation $R_{2.08} = 12.35 \pm 0.75$ km, where $R_{2.08}$ represents the radius of $2.08M_\odot$ NS [38].

In Ref. [41], the crossover between HM to QM is assumed to begin at $1.5\rho_0$, and the dependence on G_v is presented. Compared to the $R_{1.4}$ of Togashi EoS in which there are only nucleons, the NS radius becomes larger if the QM is included in the core by about 0.2–0.3 km. This behavior is opposite to the result of MS-B+vNJL in [40]. The radius of $2.08M_\odot$ NS is in the range 11.5–12 km for the G_v values that have maximum masses larger than $2.08M_\odot$. It is shown in the paper that the values of G_v must be larger than $0.84G_s$ to satisfy the condition $M_{\max} \geq 2.08M_\odot$. Also, this shows that the G_v value in Ref. [41] is much larger than the value of G_v that is obtained in our work to satisfy the $2M_\odot$. However, some recent references in the literature [42, 43] also reported that the strength of G_v is in the same order as that used in this work to give $2M_\odot$. It is worth noting that there is no stringent constraint for the values of G_v available nowadays. More precise data are needed to constrain G_v .

It is informative to compare our result of NS radius around the NS maximum mass with the NICER result in $R_{2.08} = 11.6$ – 13.1 km. With HM only, the NS radii at NS maximum mass are in the range of 9.8–11 km. The NS radii tend to increase in a stiffer EoS, giving the largest NS radius for the KIDS-C model. However, even the largest value of NS radius is relatively smaller compared to the lower limit of NICER $R_{2.08}$. The inconsistency could be understood as a signal for the existence of phases other than the hadrons. Comparing the results of KIDS-A, KIDS-B, KIDS-C, and KIDS-D models, a soft EoS of HM gives larger values of ρ_c , so even if the QM is formed in the core, R_{\max} (radius of the NS maximum mass) is too small to be consistent with the range of NICER $R_{2.08}$. The KIDS-A model clearly shows such behavior. On the other hand, stiff EoSs like the KIDS-C and D models show that the phase transition occurs at a relatively large NS radius, so the NS radius of the maximum mass is shifted to the values larger than those of pure HM. As a result, the NS with QM in the core can explain the NICER $R_{2.08}$ data better than the NSs with nucleons

only.

While the KIDS-A, KIDS-B, KIDS-C, and KIDS-D models are determined to satisfy the constraint $R_{1.4} = 11.8\text{-}12.5$ km, which is more restrictive than the NICER $R_{1.4}$, the SLy4 and KIDS0 models are fitted to the APR pure neutron matter EoS [44] in the isovector component of the functional. For this reason, the M - R behaviors of the SLy4 and KIDS0 models are similar to each other, which are not consistent with NICER $R_{1.4}$ and $R_{2.08}$.

The result of this work clearly shows that the symmetry energy plays an important role in not only controlling the stiffness of EoS of HM, but also affecting the bulk properties of the NSs with QM core. The KIDS-C and D models with G_v values larger than $0.5G_s$ satisfy the NS mass data of $1.4M_\odot$ and $2.08M_\odot$. The values of the nuclear symmetry energy parameters L and K_{sym} are respectively 58 and -91.5 MeV for the KIDS-C model, and they are 47 and -134.5 MeV for the KIDS-D model, respectively. These values are consistent with the 95 % credible range obtained from the KIDS-R14 model set [45], $L = 49.8 \pm 10.4$ MeV, and $K_{\text{sym}} = -82.4 \pm 67.4$ MeV.

IV. SUMMARY

In summary, the role of nuclear symmetry energy has been investigated in the transition from hadron matter to deconfined quark phase in the NS core. Major concerns are (i) the dependence of the critical density for the phase transition on the symmetry energy and (ii) the role of the repulsive vector coupling in the EoS of QM and NS properties. The nuclear symmetry energy is determined to satisfy the data of the canonical mass of NSs. The effect of the uncertainty due to the symmetry energy becomes obvious in the M - R relation of the NSs with masses close to $2M_\odot$.

Quark matter EoS is described in the NJL model. For a rigorous treatment of the ultraviolet divergence, we employed the PTR scheme. It is known that repulsive vector coupling is essential to reach the maximum mass of the hybrid star to be consistent with the $2M_\odot$ astrophysical observation. Dependence on the vector coupling is examined by using three different values of the vector coupling constants $G_v = 0.00, 0.25,$ and 0.50 in the unit of the G_s . Critical density for the phase transition is determined from the condition $P_{\text{HM}}(\rho_c) = P_{\text{QM}}(\rho_c)$ at $\rho_{\text{HM}} = \rho_{\text{QM}} = \rho_c$.

We found that the critical density is highly sensitive to symmetry energy. Comparing the

ρ_c values among the four models: KIDS-A, KIDS-B, KIDS-C, and KIDS-D models, the value of ρ_c tends to decrease with softer symmetry energy, i.e., $\rho_c(\text{A}) > \rho_c(\text{B}) > \rho_c(\text{C}) > \rho_c(\text{D})$ regardless of the vector coupling constant. When the vector repulsion is turned off ($G_v = 0$), the maximum mass NS is obtained about $(1.5\text{--}1.6)M_\odot$. This confirms that repulsive vector coupling is really needed for obtaining the consistency result with $2M_\odot$ observation. Since the NS maximum masses are obtained at ρ_c for $G_v = 0$, properties of the $1.4M_\odot$ NSs are not affected by the transition to QM. Therefore, the EoS of $1.4M_\odot$ NS could be determined accurately in terms of the hadronic degrees of freedom.

For $G_v = 0.25G_s$, once the QM is created in the NS core, the NS reaches the maximum mass around $1.9M_\odot$, which is quite independent of the model. To satisfy the observation, a stronger repulsion is required. With $G_v = 0.50G_s$, we found that the NS maximum mass is consistent with astrophysical observation, but the NS radius becomes inconsistent with the observation findings. For the KIDS-A and B models, the phase transition does not improve the NS M - R relation, which is out of the range of the NS radius determined by the NICER analysis. On the other hand, the KIDS-C, and D models agree with the NICER range if the QM exists in the NS core.

Consequently, we have shown that the density dependence of the symmetry energy and G_v play a critical role in the phase transition from hadron to quark matters. Critical density is sensitive to both symmetry energy and the vector coupling constant. Their effects are crucial to the M - R behavior of the hybrid stars whose masses are above the NS canonical mass. Precise measurement of the large mass of the NSs will offer a unique opportunity to constrain the symmetry energy in the HM and repulsion vector coupling in the QM simultaneously.

Acknowledgments

P.T.P.H. thanks to Daniel Whittenbury for the discussion. This work was supported by the National Research Foundation of Korea (NRF) Grant Nos. 2018R1A5A1025563, 2022R1A2C1003964, 2022K2A9A1A0609176, and 2023R1A2C1003177.

[1] S. Choi, E. Hiyama, C. H. Hyun and M. K. Cheoun, Eur. Phys. J. A **58**, no.8, 161 (2022).

- [2] C. Y. Ryu, C. H. Hyun, S. W. Hong and B. T. Kim, *Phys. Rev. C* **75**, 055804 (2007).
- [3] Y. Lim, K. Kwak, C. H. Hyun and C. H. Lee, *Phys. Rev. C* **89**, no.5, 055804 (2014).
- [4] P. Papakonstantinou, T.-S. Park, Y. Lim and C. H. Hyun, *Phys. Rev. C* **97**, no.1, 014312 (2018).
- [5] H. Gil, P. Papakonstantinou, C. H. Hyun and Y. Oh, *Phys. Rev. C* **99**, no.6, 064319 (2019).
- [6] H. Gil, Y.-M. Kim, C. H. Hyun, P. Papakonstantinou and Y. Oh, *Phys. Rev. C* **100**, no.1, 014312 (2019).
- [7] H. Gil, Y.-M. Kim, P. Papakonstantinou and C. H. Hyun, *Phys. Rev. C* **103**, no.3, 034330 (2021).
- [8] H. Gil and C. H. Hyun, *New Phys.: Sae Mulli* **71**, no.3, 242-248 (2021).
- [9] H. Gil, P. Papakonstantinou and C. H. Hyun, *Int. J. Mod. Phys. E* **31**, no.01, 2250013 (2022).
- [10] P. T. P. Hutaeruk, H. Gil, S. i. Nam and C. H. Hyun, *Phys. Rev. C* **106**, no.3, 035802 (2022).
- [11] P. T. P. Hutaeruk, H. Gil, S. i. Nam and C. H. Hyun, *PTEP* **2023**, no.6, 063D01 (2023).
- [12] P. Danielewicz, R. Lacey and W. G. Lynch, *Science* **298**, 1592-1596 (2002).
- [13] I. Tews, T. Krüger, K. Hebeler and A. Schwenk, *Phys. Rev. Lett.* **110**, no.3, 032504 (2013).
- [14] J. Antoniadis, P. C. C. Freire, N. Wex, T. M. Tauris, R. S. Lynch, M. H. van Kerkwijk, M. Kramer, C. Bassa, V. S. Dhillon and T. Driebe, *et al. Science* **340**, 6131 (2013).
- [15] H. T. Cromartie *et al.* [NANOGrav], *Nature Astron.* **4**, no.1, 72-76 (2019).
- [16] P. Demorest, T. Pennucci, S. Ransom, M. Roberts and J. Hessels, *Nature* **467**, 1081-1083 (2010).
- [17] P. T. P. Hutaeruk and S. i. Nam, *Phys. Rev. D* **105**, no.3, 3 (2022).
- [18] T. Tanimoto, W. Bentz and I. C. Cloët, *Rev. C* **101**, no.5, 055204 (2020).
- [19] P. T. P. Hutaeruk and S. i. Nam, *Mod. Phys. Lett. A* **37**, no.14, 2250087 (2022).
- [20] W. Bentz and A. W. Thomas, *Nucl. Phys. A* **696**, 138-172 (2001).
- [21] G. Baym, T. Hatsuda, T. Kojo, P. D. Powell, Y. Song, and T. Takatsuka, *Rept. Prog. Phys.* **81**, no.5, 056902 (2018).
- [22] M. Buballa, *Phys. Rept.* **407**, 205-376 (2005).
- [23] N. K. Glendenning, *Phys. Rev. D* **46**, 1274-1287 (1992).
- [24] P. T. P. Hutaeruk, [arXiv:2204.11520 [hep-ph]].
- [25] P. T. P. Hutaeruk, I. C. Cloet and A. W. Thomas, *Phys. Rev. C* **94**, no.3, 035201 (2016).
- [26] P. T. P. Hutaeruk, W. Bentz, I. C. Cloët and A. W. Thomas, *Phys. Rev. C* **97**, no.5, 055210

- (2018).
- [27] J. S. Schwinger, Phys. Rev. **82**, 664-679 (1951)
 - [28] T. Hell and W. Weise, Phys. Rev. C **90**, no.4, 045801 (2014).
 - [29] S. Klimt, M. F. M. Lutz and W. Weise, Phys. Lett. B **249**, 386-390 (1990).
 - [30] S. Lawley, W. Bentz and A. W. Thomas, Phys. Lett. B **632**, 495-500 (2006).
 - [31] G. Ripka, “Quarks bound by chiral fields: The quark-structure of the vacuum and of light mesons and baryons” (Oxford University Press, Oxford, 1997).
 - [32] R. L. Workman *et al.* [Particle Data Group], PTEP **2022**, 083C01 (2022).
 - [33] J. R. Oppenheimer and G. M. Volkoff, Phys. Rev. **55**, 374-381 (1939).
 - [34] R. C. Tolman, Phys. Rev. **55**, 364-373 (1939).
 - [35] R. C. Tolman, Proc. Nat. Acad. Sci. **20**, 169-176 (1934).
 - [36] J. Macher and J. Schaffner-Bielich, Eur. J. Phys. **26**, 341-360 (2005).
 - [37] T. Endo, Phys. Rev. C **83**, 068801 (2011).
 - [38] M. C. Miller, *et al.*, Astrophys. J. Lett. **918**, L28 (2021).
 - [39] S. Choi, E. Hiyama, C. H. Hyun, and M.-K. Cheoun, in progress.
 - [40] S. Han, M. A. A. Mamun, S. Lalit, C. Constantinou, and M. Prakash, Phys. Rev. D **100**, 103022 (2019).
 - [41] T. Kojo, G. Baym, and T. Hatsuda, Astrophys. J. **934**, 46 (2022).
 - [42] G. B. Alaverdyan, Astrophysics **65**, no.2, 278-295 (2022).
 - [43] A. Kumar, V. B. Thapa and M. Sinha, Phys. Rev. D **107**, no.6, 063024 (2023)
 - [44] A. Akmal, V. R. Pandharipande, and D. G. Ravenhall, Phys. Rev. C **58**, 1804 (1998).
 - [45] C. H. Hyun, New Phys.: Sae Mulli **72**, no.5, 371-375 (2022).